Asian Journal of Andrology (2017) 19, 439–443
www.asiaandro.com; www.ajandrology.com

Open Access

ORIGINAL ARTICLE

Prostatic Diseases

Detecting prostate cancer and prostatic calcifications using advanced magnetic resonance imaging

Shewei Dou[1,*], Yan Bai[1,*], Ankit Shandil[2], Degang Ding[3], Dapeng Shi[1], E Mark Haacke[4,5], Meiyun Wang[1]

Prostate cancer and prostatic calcifications have a high incidence in elderly men. We aimed to investigate the diagnostic capabilities of susceptibility-weighted imaging in detecting prostate cancer and prostatic calcifications. A total number of 156 men, including 34 with prostate cancer and 122 with benign prostate were enrolled in this study. Computed tomography, conventional magnetic resonance imaging, diffusion-weighted imaging, and susceptibility-weighted imaging were performed on all the patients. One hundred and twelve prostatic calcifications were detected in 87 patients. The sensitivities and specificities of the conventional magnetic resonance imaging, apparent diffusion coefficient, and susceptibility-filtered phase images in detecting prostate cancer and prostatic calcifications were calculated. McNemar's Chi-square test was used to compare the differences in sensitivities and specificities between the techniques. The results showed that the sensitivity and specificity of susceptibility-filtered phase images in detecting prostatic cancer were greater than that of conventional magnetic resonance imaging and apparent diffusion coefficient ($P < 0.05$). In addition, the sensitivity and specificity of susceptibility-filtered phase images in detecting prostatic calcifications were comparable to that of computed tomography and greater than that of conventional magnetic resonance imaging and apparent diffusion coefficient ($P < 0.05$). Given the high incidence of susceptibility-weighted imaging (SWI) abnormality in prostate cancer, we conclude that susceptibility-weighted imaging is more sensitive and specific than conventional magnetic resonance imaging, diffusion-weighted imaging, and computed tomography in detecting prostate cancer. Furthermore, susceptibility-weighted imaging can identify prostatic calcifications similar to computed tomography, and it is much better than conventional magnetic resonance imaging and diffusion-weighted imaging.

Asian Journal of Andrology (2017) **19**, 439–443; doi: 10.4103/1008-682X.177840; published online: 22 March 2016

Keywords: calcification; computed tomography; diffusion-weighted imaging; magnetic resonance imaging; prostate cancer; susceptibility-weighted imaging

INTRODUCTION

Prostate cancer and prostatic calcifications are commonly found in elderly men.[1–3] Among men, prostate cancer accounts for about 28% of newly diagnosed cancers.[4] Previous studies suggested that foci of prostate hemorrhages were relevant to prostate cancers, and prostatic calcifications were present in some urological diseases and symptoms.[3,5–7] Computed tomography (CT) is thought to be the gold standard in detecting calcifications,[8] but it has very little use in detecting prostate cancer.[9] Conventional magnetic resonance imaging (MRI), which provides higher soft-tissue differentiation, has been more widely used than CT for the clinical examination of the prostate. However, it has limited sensitivities and specificities in detecting prostate cancer and prostatic calcifications.[2,10,11] Diffusion-weighted imaging (DWI) is a noninvasive MRI technique that provides information on the diffusion of water molecules in the biological tissues. As a supplement to conventional MRI, the apparent diffusion coefficient (ADC) map obtained from DWI could improve the diagnosis of prostate cancer.[12] However, values for prostate cancer and benign prostate have overlaps on the ADC maps.[12]

With the development of advanced MRI techniques such as susceptibility-weighted imaging (SWI), which reflects the magnetic susceptibility of tissues,[13] hemorrhages and calcifications can be detected in a noninvasive way by using susceptibility-filtered phase images.[14–16] However, to our knowledge, no study has been performed to compare conventional MRI, DWI, and SWI in detecting prostate cancer and prostatic calcifications. The purpose of this study was to evaluate and compare the capabilities of conventional MRI, DWI, and SWI in detecting prostate cancer and prostatic calcifications.

MATERIALS AND METHODS

Study participants

This study was approved by the local Institutional Review Board, and written informed consent was obtained from each subject before

[1]Department of Radiology, Henan Provincial People's Hospital and The People's Hospital of Zhengzhou University, Zhengzhou 450003, Henan, China; [2]Department of Postgraduate Education, School of International Education, Zhengzhou University, Zhengzhou 450001, Henan, China; [3]Department of Urology, Henan Provincial People's Hospital and The People's Hospital of Zhengzhou University, Zhengzhou 450003, Henan, China; [4]Department of Radiology, Wayne State University, Detroit 48202, MI, USA; [5]Department of Administration, Magnetic Resonance Innovations Inc., Detroit 48202, USA.
*These authors contributed equally to this work.
Correspondence: Dr. M Wang (mywang@ha.edu.cn)
Received: 14 May 2015; Revised: 14 July 2015; Accepted: 21 January 2016

participation. A total number of 156 men with prostatic diseases (age range 56–83 years, average age 67 years), including 34 patients with prostate cancers and 122 patients with benign prostates, between June 2011 and October 2014, were enrolled in this study. The inclusion criteria were as follows: (a) the prostate-specific antigen (PSA) levels of the patients were higher than 4.0 ng ml^{-1} within 1 week, before the CT and MRI examinations; (b) both CT and MRI examinations were performed on all the subjects before performing biopsies of the prostate; and (c) the histopathological diagnoses, based on the World Health Organization 2007 criteria were achieved from the biopsies of the prostate. The exclusion criteria were the following: (a) history of biopsy, surgery, radiotherapy, transurethral resection, brachytherapy, or trauma to the prostate, before CT and MRI scanning; (b) unavailability of MRI data due to movement artifact. Prostate cancer and a benign prostate were diagnosed by histopathologic results of transrectal ultrasound-guided biopsies after performing the CT and MRI examinations. In 87 of the 156 patients, 112 prostatic calcifications were detected by using CT images, which is the gold standard. This study was approved by the local Institutional Review Board. Written, informed consent was obtained from every patient before participation.

Computed tomography protocol

Axial CT without contrast was performed on a 16-row multi-slices CT scanner with a tube voltage of 120 kV, a tube current of 250 mA, and a slice thickness of 3 mm.

Magnetic resonance imaging protocols

Conventional MRI without contrast, DWI, and high-resolution SWI were performed on a 3T scanner with a pelvic array-phased coil. T1-weighted image (T1WI) had a field of view (FOV) of 300 mm × 300 mm, a matrix of 288 × 320, a repetition time (TR) of 700 ms, an echo time (TE) of 11 ms, a flip angle of 150°, and a slice thickness of 3 mm. The acquisition time was 3 min and 25 s. T2-weighted image (T2WI) had a FOV of 300 mm × 300 mm, a matrix of 272 × 320, a TR of 4000 ms, a TE of 87 ms, a flip angle of 140°, and a slice thickness of 3 mm. The acquisition time was 3 min and 54 s.

DWI was obtained using a single-shot, echo-planar sequence with a TR of 4500 ms, a TE of 79 ms, a FOV of 300 mm × 300 mm, a matrix of 192 × 154, and a slice thickness of 3 mm. Two b values of 0 and 800 s mm^{-2} (7 averages) were used in three diffusion directions. The acquisition time was 2 min and 20 s. The ADC map was calculated from the b values of 0 and 800 s mm^{-2} by a mono-exponential model as follows:[17] $S(b)/S(0) = \exp(-b \times ADC)$, where S(b) represents the signal intensity in the presence of diffusion sensitization and S(0) represents the signal intensity in the absence of diffusion sensitization.

SWI was a three-dimensional, fast, low-angle gradient-echo (GRE) sequence with a FOV of 300 mm × 300 mm, a matrix of 512 × 282, a TR of 22 ms, a TE of 12 ms, a flip angle of 20°, and a slice thickness of 3 mm. The acquisition time was 3 min and 36 s. Axial conventional MRI was performed with fast spin-echo (FSE) sequences. The susceptibility phase image was obtained from SWI. It was high pass filtered with a 64 × 64 exclusion of low-spatial frequency information. A phase mask was created by setting all positive phase values (between 0° and 180°) to unity and normalizing the negative-phase values ranging from 0° to 180° to a gray scale of values ranging linearly from 1 to 0, respectively.

Prostate biopsy protocol

The patients underwent initial biopsies of the prostate within 10 days after the completion of the CT and MR examinations. The initial sextant biopsies were performed at the base, middle, and apex of the prostate, on both sides. In the initial biopsies, some patients had at least two additional biopsies taken in areas suspected of prostate cancer, as defined by the MRI examinations. When the initial biopsies of the prostate were done, the patients with an initial negative biopsy result had repeated tests of PSA, 4–6 weeks later. Biopsies were repeated in patients who had PSA levels of more 10.0 ng ml^{-1}. Extended sextant biopsies with 14 biopsy cores were performed within 10 days, after the completion of the repeat PSA tests. All the biopsy cores were labeled according to the location of the prostate.

Data analysis

Two radiologists (YB and MW, with 8 and 19 years' of diagnostic experiences, respectively), who were blinded to the histopathologic results of patients, independently reviewed all the CT, conventional MRI, ADC, and susceptibility-filtered phase images to detect abnormalities that were suspected to be hemorrhages, cancers, and calcifications in the prostate. They identified abnormalities which were suspected to be hemorrhages by the means of hyperintense signals on T1-weighted images, hypointense signals on ADC maps and susceptibility-filtered phase images, and high density on CT images. The radiologists diagnosed prostate cancer by combining the findings of hypointense signals on T2-weighted images and ADC maps, hypointense abnormalities on susceptibility-filtered phase images, and lumps on CT images. The calcifications were defined by a dot-like hypointense signals on T2-weighted images, hyperintense signals on susceptibility-filtered phase images, hypointense signals on ADC maps, and ultra-high density on CT images. The discrepancies between the two radiologists in regard to the entire analyses except that of CT were settled with a consensus review by a third radiologist (DS with 31 years' of diagnostic experience). The two radiologists (YB and MW) independently measured the length-diameters of hypointense abnormalities on susceptibility-filtered phase images. CT results were taken as the gold standard for detecting prostatic calcifications, which were confirmed by viewing over 100 Hounsfield units of CT.[8] The units of CT and the volumes of prostate were measured on the workstation (Philips Medical Systems, Eindhoven, The Netherlands).

Statistical analysis

The Mann–Whitney U-tests were used to compare the ages, prostate sizes, and levels of PSA before the CT and MRI examinations, between patients with prostate cancers and patients with benign prostate. Sensitivities and specificities for conventional MRI, ADC, and susceptibility-filtered phase images in detecting prostate cancer and prostatic calcifications were calculated. The sensitivity and specificity for detecting calcifications were on a per-lesion basis, whereas the sensitivity and specificity for determining prostate cancer were on a per-subject basis. McNemar's Chi-square test was used to compare the differences in detections by the two radiologists (YB and MW) and the differences in sensitivities and specificities between the different imaging techniques.

RESULTS

Table 1 compares the characteristics of patients with prostate cancer and patients with benign prostate. There were no differences in the ages and prostate sizes ($P = 0.31$) between the patients with prostate cancer and the patients with benign prostate. The levels of PSA before the examinations were significantly higher ($P < 0.001$) in patients with prostate cancer than those in patients with benign prostate. Prostate cancer that was diagnosed by histopathologic examination of biopsies was located in the peripheral zones of the prostate. In the initial biopsies, 55 patients underwent at least two additional biopsies in the areas suspected of prostate cancer. Twenty-nine patients were

diagnosed with prostate cancer by the initial biopsies. Nineteen patients had repeated, extended sextant biopsies with 14 biopsy cores, five of which were diagnosed as prostate cancer. In 30 out of the 34 patients (88%) with prostate cancer, hypointense abnormalities were detected in the areas of prostate cancer on the susceptibility-filtered phase images (**Figure 1**). As compared to SWI (sensitivity 88% and specificity 100%), conventional MRI (sensitivity 27% and specificity 68%, $P < 0.001$) and ADC maps (sensitivity 33% and specificity 66%, $P < 0.001$) had less value in detecting abnormalities which were suspected to be hemorrhages, and CT could not detect any hemorrhages in the prostate cancer (**Figure 1**). Abnormalities suspected to be hemorrhages were not detected in patients with benign prostate by using CT, conventional MRI, DWI, and SWI. Hence, the hypointense abnormalities detected by susceptibility-filtered phase images were more commonly seen in patients with prostate cancers (88%) than in those with a benign prostate (0%). The average over length-diameters of hypointense abnormalities detected by susceptibility-filtered phase images in the prostate by the two radiologists was 3.9 mm and 3.6 mm, respectively. The sensitivity and specificity for susceptibility-filtered phase images (88% and 100%) in the diagnoses of prostate cancer were greater than those for conventional MRI (71% and 77%, $P = 0.03$ and $P < 0.001$, respectively) and ADC images (74% and 79%, $P = 0.03$ and $P < 0.001$, respectively).

A total of 112 prostatic calcifications (101 calcifications in the central zones and 11 calcifications in the peripheral zones) were detected on CT images in 87 patients (6 patients with prostate cancer and 81 patients with benign prostatic disease) (**Supplementary Table 1**). Compared to CT, the sensitivity and specificity for susceptibility-filtered phase images (97% and 100%) in detecting prostatic calcifications were greater than those for conventional MRI (32% and 91%) and ADC images (38% and 88%), ($P < 0.001$) (**Figure 2**).

Table 1: Comparison of characteristics between the patients with prostate cancer and patients with benign prostate

Characteristics	*Patients with prostate cancers*	*Patients with benign prostates*	*P*
n	34	122	-
Percentage	22	78	-
Age, in years (mean±s.d.)	69±7	67±6	0.22
Prostate volume, ml (mean±s.d.)	39.2±12.7	37.8±13.4	0.31
Levels of PSA, ng ml^{-1} (mean±s.d.)	21.8±12.3	4.9±0.7	<0.00
Number of prostatic calcifications	7	105	-

s.d.: standard deviation; PSA: prostate-specific antigen; -: not applicable

The sensitivity and specificity of susceptibility-filtered phase images were higher than those of the other imaging techniques in all the analyses ($P < 0.05$). There were no discrepancies in regard to diagnosing the presence of abnormalities on the susceptibility-filtered phase images and the number of hemorrhages and calcifications on CT images, between the two radiologists (YB and MW). There were no differences in the detection of abnormalities between the two radiologists (YB and MW) ($P = 0.32$).

DISCUSSION

Conventional MRI is useful in detecting prostate cancer, but it has limited sensitivity and specificity.[2] Prostate cancer in the peripheral zone could be identified by the presence of hypointensity on T2WI. However, the hypointensity on T2WI could also be found in prostatitis and fibrosis.[18] In addition, ADC map obtained from DWI improves the prediction of prostate cancer, as a supplement to T2WI. ADC value is generally lower in prostate cancer as compared to that in benign prostate because water molecular diffusion is greatly restricted in prostate cancer due to a high cellular density.[2,19] However, there are overlaps in the ADC values of the cancerous and benign tissues in the prostate.[12] Consequently, it is desirable to develop other MRI techniques to improve the detections of prostate cancer.

Susceptibility-weighted imaging (SWI) is a new noninvasive MRI technique which is sensitive to paramagnetic materials such as deoxygenated blood, blood products, and iron.[20,21] Although SWI is a widely accepted tool in detecting microbleeds and calcifications in the brain,[14–16] the value of SWI in detecting microbleeds and calcifications in prostatic diseases has not been investigated. In the present study, we assessed the values of susceptibility-filtered phase images obtained from SWI in detecting abnormalities by comparing it with that of DWI and conventional MRI. Our results demonstrated that most cases of prostate cancer were detected by hypointense abnormalities in the lesions of prostate cancer by susceptibility-filtered phase images (88%), whereas no hypointense abnormality was detected in patients with benign prostate (0%). The hypointense abnormalities on susceptibility-filtered phase images have been shown to correlate with the hemorrhages,[16,20] and our results indicated that those focal abnormalities were associated with prostate cancer. Thus, the hypointense abnormalities on susceptibility-filtered phase images of prostate should be a good biomarker for the diagnosis of prostate cancer. The rationale for this is that prostate cancer has a higher microvessel density than the benign tissue of the prostate.[22] The microvessels in the areas of prostate cancer are more fragile and

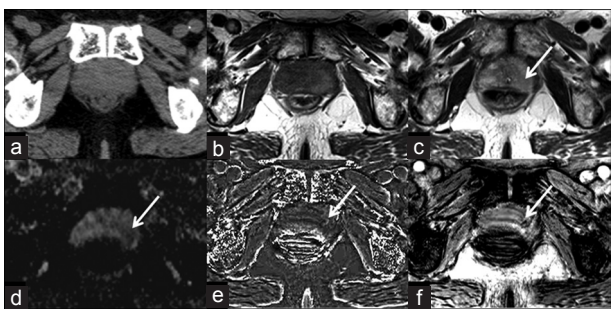

Figure 1: An 81-year-old male with prostate cancer in the left peripheral zone. Prostate cancer and hemorrhage are not displayed on the CT image (**a**), isointensity on T1WI (**b**), iso- to hypointensity on T2WI (**c**) and ADC map (**d**). Arrows indicate the areas of prostate cancer. Hypointensity on susceptibility-filtered phase images (**e**), and susceptibility-weighted image (**f**) (arrows), prove the micro-abnormality of prostate cancer.

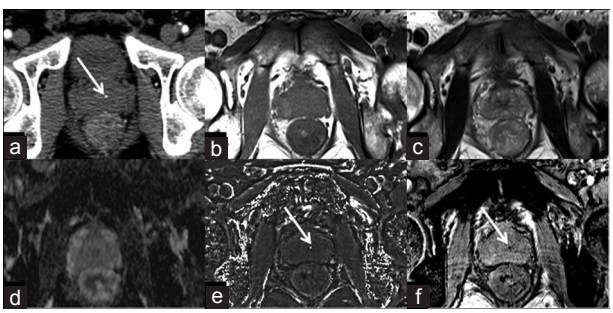

Figure 2: A 58-year-old male with calcification in the central zone of prostate. Prostatic calcification is seen as a dot-like high-density spot on the CT image (**a**) (arrow), but is hard to be identified on conventional T1WI (**b**), T2WI (**c**), and ADC map (**d**). Hyperintensity on susceptibility-filtered phase images (**e**) and hypointensity on susceptibility-weighted image (**f**) (arrows) indicate calcification.

irregular than those in the benign tissues of the prostate.[22] Therefore, prostate cancer tissues are prone to bleeding unlike the benign tissues of prostate. Our results would provide a useful and noninvasive tool for the detection of prostate cancer, thereby avoiding an invasive biopsy. However, in postbiopsy patients with prostate cancer, Barrett *et al*.[23] found that the hemorrhage caused by biopsy was obviously less in the areas of prostate cancer than in the region of benign prostate. This result may be explained by the reduced level of anticoagulant effect of citrate in the areas of prostate cancer, which causes any hemorrhages present in the tumor foci to resolve more rapidly than the hemorrhages in the normal peripheral zone.[23] Hence, the history of biopsy is very important for determining the cause of hemorrhage, detected by MRI. Furthermore, our results showed that SWI would be valuable for the early and accurate diagnosis of prostate cancer before an invasive biopsy. In the present study, we found that the sizes of the hypointense abnormalities on the susceptibility-filtered phase images of prostate cancer were generally small and were hard to be detected by the other imaging techniques. In our study, conventional MRI and ADC images had less potential in detecting abnormalities which were suspected to be hemorrhages than that of SWI, and CT could not detect any hemorrhages in prostate cancer. Hence, SWI is much more sensitive in detecting the abnormalities of prostate cancer than conventional MRI, DWI, and CT. Thus, it can be used as a noninvasive and useful tool for the early detection of prostate cancer, and in improving the prognosis. Our results revealed higher sensitivity and specificity for susceptibility-filtered phase images (88% and 100%) in the diagnoses of prostate cancer than that of ADC maps derived from DWI (76% and 79%).

SWI is also sensitive to diamagnetic substances such as calcifications, which have specific magnetic susceptibility differences relative to the background or surrounding tissues.[13,20] CT has been thought to be the gold standard in detecting calcifications.[8] Currently, similar to CT, susceptibility-filtered phase images have become a reliable method to detect intracranial calcifications.[14,15] Prostatic calcifications can be found in men with benign prostatic hyperplasia, prostate cancer, prostatitis, and chronic prostatitis/chronic pelvic pain syndrome (CPPS).[3,13,24] Conventional MRI is more commonly used for prostatic examination than CT because of its higher soft-tissue differentiation. However, as the signal intensity of prostatic calcification on conventional MRI is varied due to the complicated components and various proportions in calcification, prostatic calcification is difficult to be detected by a conventional MRI. In addition, most calcifications in the prostate are small in size, which makes it hard to be detected by a conventional MRI. In susceptibility-filtered phase images, the small calcifications show sharp boundaries, which provide a high contrast between the calcifications and the surrounding tissues.[14] Thus, our results from a large sample size proved that susceptibility-filtered phase images could identify prostatic calcifications comparable to CT, and had a far higher sensitivity than conventional MRI and ADC images. The pathogenesis of prostatic calcification has been largely unclear so far. Nevertheless, it is assumed to be formed by the precipitations of prostatic secretions and in conditions of inflammations.[25] Although the clinical significances of prostatic calcifications related with prostatic diseases were ambiguous, some studies indicated that prostatic calcifications were associated with several urological diseases and symptoms. Hong *et al*.[6] reported that prostatic calcifications could aggravate lower urinary tract symptoms because prostatic calcification affected the mechanical obstruction and smooth muscle contraction in the prostate and the bladder neck. Kirby *et al*.[26] suggested that the reflux of urine in chronic prostatitis could be associated with the formation of prostatic calcification. Shoskes *et al*.[27] claimed that prostatic calcification was related to infection, bacterial colonization, and the duration of symptoms in patients with CPPS. Moreover, as a reliable marker, prostatic calcification can be useful for a precise location of image-guided radiation therapy.[28,29] Consequently, accurate detections of prostatic calcifications have various clinical applications.

The other advantage of susceptibility-weighted imaging over DWI is that, it can distinguish calcification from hemorrhage by using the susceptibility-filtered phase image, whereas both calcification and hemorrhage show hypointensity on DWI. Susceptibility-filtered phase image is especially sensitive to the differences in local magnetic susceptibility, which can be induced by both a calcification and a hemorrhage.[30] Fortunately, the paramagnetic and diamagnetic materials have opposite signal intensities in susceptibility-filtered phase images because the magnetic susceptibility is <0 in diamagnetic materials, whereas >0 in paramagnetic substances.[15] In general, calcification shows a high signal or a mixed signal dominated by high signal, but hemorrhage displays a low signal or a mixed signal dominated by low signal on susceptibility-filtered phase images.[16] Thus, a hemorrhage can be easily distinguished from a calcification in a susceptibility-filtered phase image.

There were some limitations in our study. First, the histopathologic results were acquired by biopsies instead of prostate resection. Thus, the hypointense abnormalities that appeared on the susceptibility-filtered phase images were not directly proved to be hemorrhages. A confirmation by histopathology studies should be acquired in the future studies. Second, cancer areas were located in the peripheral zones of the prostate in this study. Third, the DWI protocol of this study did not include low b values to reflect the perfusion characteristics of prostate cancer. In addition, the connections between prostatic calcifications and symptoms/complaints of urological were not investigated in this study. Further studies of SWI in the prostate cancer of the central zones and the relevance between prostatic calcifications and symptoms of urological diseases should be performed in the future.

CONCLUSION

SWI has both a higher sensitivity and specificity than conventional MRI and DWI in detecting prostate cancer. Furthermore, SWI can identify prostatic calcification comparable to CT, and it is much better than conventional MRI and DWI.

AUTHOR CONTRIBUTIONS

SD, YB, AS, DD, EMK, and MW planned, coordinated, and conducted the study. SD, YB, DS, and MW analyzed the data and performed the statistical study. SD, YB, and MW wrote and revised the manuscript. MW received research grants from China and supervised the project. All authors read and approved the final manuscript.

COMPETING INTERESTS

All authors declare no competing interests.

ACKNOWLEDGMENTS

This study was supported in part by the National Natural Science Foundation of China (No. 81271565 and 31470047), the Distinguished Young Scholar in Scientific and Technical Innovation Foundation of Henan Province, China (No. 124100510016), the Science and Technology Foundation of Public Health of Henan Province, China (No. 201202018 and 201003095).

Supplementary information is linked to the online version of the paper on the *Asian Journal of Andrology* website.

REFERENCES

1 Zhu Y, Wang HK, Qu YY, Ye DW. Prostate cancer in East Asia: evolving trend over the last decade. *Asian J Androl* 2015; 17: 48–57.
2 Choi YJ, Kim JK, Kim N, Kim KW, Choi EK, *et al*. Functional MR imaging of prostate cancer. *Radiographics* 2007; 27: 63–75.
3 Klimas R, Bennett B, Gardner WA. Prostatic calculi: a review. *Prostate* 1985; 7: 91–6.
4 Siegel R, Naishadham D, Jemal A. Cancer statistics, 2013. *CA Cancer J Clin* 2013; 63: 11–30.
5 Bai Y, Wang MY, Han YH, Dou SW, Lin Q, *et al*. Susceptibility weighted imaging: a new tool in the diagnosis of prostate cancer and detection of prostatic calcification. *PloS One* 2013; 8: e53237.
6 Hong CG, Yoon BI, Choe HS, Ha US, Sohn DW, *et al*. The prevalence and characteristic differences in prostatic calcification between health promotion center and urology department outpatients. *Korean J Urol* 2012; 53: 330–4.
7 Park SW, Nam JK, Lee SD, Chung MK. Are prostatic calculi independent predictive factors of lower urinary tract symptoms. *Asian J Androl* 2010; 12: 221–6.
8 Kucharczyk W, Henkelman RM. Visibility of calcium on MR and CT: can MR show calcium that CT cannot? *AJNR Am J Neuroradiol* 1994; 15: 1145–8.
9 Hricak H, Choyke PL, Eberhardt SC, Leibel SA, Scardino PT. Imaging prostate cancer: a multidisciplinary perspective. *Radiology* 2007; 243: 28–53.
10 Avrahami E, Cohn DF, Feibel M, Tadmor R. MRI demonstration and CT correlation of the brain in patients with idiopathic intracerebral calcification. *J Neurol* 1994; 241: 381–4.
11 Tsuchiya K, Makita K, Furui S, Nitta K. MRI appearances of calcified regions within intracranial tumours. *Neuroradiology* 1993; 35: 341–4.
12 Lim HK, Kim JK, Kim KA, Cho KS. Prostate cancer: apparent diffusion coefficient map with T2-weighted images for detection – A multireader study. *Radiology* 2009; 250: 145–51.
13 Haacke EM, Xu Y, Cheng YC, Reichenbach JR. Susceptibility weighted imaging (SWI). *Magn Reson Med* 2004; 52: 612–8.
14 Wu Z, Mittal S, Kish K, Yu Y, Hu J, *et al*. Identification of calcification with MRI using susceptibility-weighted imaging: a case study. *J Magn Reson Imaging* 2009; 29: 177–82.
15 Berberat J, Grobholz R, Boxheimer L, Rogers S, Remonda L, *et al*. Differentiation between calcification and hemorrhage in brain tumors using susceptibility-weighted imaging: a pilot study. *AJNR Am J Neuroradiol* 2014; 202: 847–50.
16 Zhu WZ, Qi JP, Zhan CJ, Shu HG, Zhang L, *et al*. Magnetic resonance susceptibility weighted imaging in detecting intracranial calcification and hemorrhage. *Chin Med J (Engl)* 2008; 121: 2021–5.
17 Le Bihan D, Breton E, Lallemand D, Aubin ML, Vignaud J, *et al*. Separation of diffusion and perfusion in intravoxel incoherent motion MR imaging. *Radiology* 1988; 168: 497–505.
18 Ikonen S, Kivisaari L, Tervahartiala P, Vehmas T, Taari K, *et al*. Prostatic MR imaging. *Acta Radiol* 2001; 42: 348–54.
19 Mazaheri Y, Hricak H, Fine SW, Akin O, Shukla-Dave A, *et al*. Prostate tumor volume measurement with combined T2-weighted imaging and diffusion-weighted MR: correlation with pathologic tumor volume. *Radiology* 2009; 252: 449–57.
20 Haacke EM, Mittal S, Wu Z, Neelavalli J, Cheng YC. Susceptibility-weighted imaging: technical aspects and clinical applications, part 1. *AJNR Am J Neuroradiol* 2009; 30: 19–30.
21 Wang M, Dai Y, Han Y, Haacke EM, Dai J, *et al*. Susceptibility weighted imaging in detecting hemorrhage in acute cervical spinal cord injury. *Magn Reson Imaging* 2011; 29: 365–73.
22 Stefanou D, Batistatou A, Kamina S, Arkoumani E, Papachristou DJ, *et al*. Expression of vascular endothelial growth factor (VEGF) and association with microvessel density in benign prostatic hyperplasia and prostate cancer. *In Vivo* 2004; 18: 155–60.
23 Barrett T, Vargas HA, Akin O, Goldman DA, Hricak H. Value of the hemorrhage exclusion sign on T1-weighted prostate MR images for the detection of prostate cancer. *Radiology* 2012; 263: 751–7.
24 König JE, Senge T, Allhoff EP, König W. Analysis of the inflammatory network in benign prostate hyperplasia and prostate cancer. *Prostate* 2004; 58: 121–9.
25 Sfanos KS, Wilson BA, De Marzo AM, Isaacs WB. Acute inflammatory proteins constitute the organic matrix of prostatic corpora amylacea and calculi in men with prostate cancer. *Proc Natl Acad Sci U S A* 2009; 106: 3443–8.
26 Kirby R, Lowe D, Bultitude MI, Shuttleworth KE. Intra-prostatic urinary reflux: an aetiological factor in a bacterial prostatitis. *Br J Urol* 1982; 54: 729–31.
27 Shoskes DA, Lee CT, Murphy D, Kefer J, Wood HM. Incidence and significance of prostatic stones in men with chronic prostatitis/chronic pelvic pain syndrome. *Urology* 2007; 70: 235–8.
28 Hama Y. Detection of prostate calcification with megavoltage helical CT. *Acad Radiol* 2014; 21: 565–8.
29 Kupelian PA, Langen KM, Willoughby TR, Zeidan OA, Meeks SL, *et al*. Image-guided radiotherapy for localized prostate cancer: treating a moving target. *Semin Radiat Oncol* 2008; 18: 58–66.
30 Mittal S, Wu Z, Neelavalli J, Haacke EM. Susceptibility-weighted imaging: technical aspects and clinical applications, part 2. *AJNR Am J Neuroradiol* 2009; 30: 232–52.